Chapter 8

Effect of non-linearity on the performance of the elaborated model

IN the previous chapter, the Dror's elaborated Reichardt model [Dror et al., 2000] was expanded and feedback adaptation and saturation was included in the model. In this chapter, a comparative study is carried out on the effects of the addition of each elaboration on the performance of the model. The relative error in each case is also studied.

8.1 Relative error

The error measure used here called the relative error defined by Dror as,

$E_{\text{rel}} = E_{\text{abs}}/\overline{R}$, where the absolute error (E_{abs}) is the difference between the actual response and the expected response [Dror, 1998]. The expected response is the mean response value that is given by $\overline{R}$. For a given set of images, moving at a given velocity, the mean response $\overline{R}$ is calculated by averaging the response of the wide field correlator at all points in the selected sampled space and sampled time. The relative error for the same set of responses is found by dividing their standard deviation by the mean. In this paper, the performance of the model is evaluated based on its effect on pattern noise.

The natural images used for evaluating the performance of our model is shown in Figure 8.1.

8.2 Role of additional components

8.2.1 Spatial pre-filtering

Studies on photo-transduction in insects reveal that the retinal signal, as sampled by the photoreceptor, is already blurred by diffraction effects of the lens optics as well as the properties of the photoreceptor themselves [Snyder et al., 1977]. Hence the response of the photoreceptor to an input image has the characteristics of spatial low pass filter. Studies and analysis by Dror (1998) suggests that low pass spatial filtering dramatically decreases the relative error of the correlator particularly at lower velocities. But at higher velocities, the relative error rises even in the presence of spatial filtering because spatial frequencies passed by the pre-filter generate high-frequency inputs to the correlator. The spatial low pass filters are found to raise the peak response velocity. Based on these studies, a spatial low pass filter is implemented in the model. While some LMCs also appear to perform spatial high-pass filtering of their inputs the phenomenon is weaker and more variable than high pass temporal filtering [James, 1990; Laughlin, 1994].

Spatial pre-filtering in our model is implemented by two-dimensional convolution of the image with a Gaussian kernel of half width of 2°, which approximates the acceptance function of typical fly photoreceptor [Hardie, 1985].

Image 1

Image 2

Image 3

Image 4

Figure 8.1. The panoramic natural images given as stimulus to the EMD model. A panorama of the image is formed by 'warping' 12 image tiles at 30° intervals to remove lens distortions and then by wrapping its ends together using Apple Quicktime VR software on a Macintosh computer.

8.2.2 Temporal pre-filtering

At very high velocities, the relative error begins to rise even in the presence of spatial pre-filtering, because the spatial frequencies passed by the pre-filter generate high temporal frequency inputs to the correlator while the steady state (DC) response declines due to the low pass nature of the EMD delay filter. Temporal pre-filtering which filters out such frequencies regardless of velocity, serves to reduce the relative error at very high motion velocities. The temporal low pass filtering is found to lower the peak response velocity where as high pass temporal filtering shifts the velocity response to the right, raising the peak velocity [Dror, 1998]. Photoreceptors, which provide the inputs to the correlator,

depend on chemical transduction processes that cannot respond instantly to changes in the luminance signal. They therefore filter their inputs with a temporal response found to experimentally to have a log-normal form [Payne and Howard, 1981]. In addition, there is clear evidence that some kind of temporal high-pass filtering takes place in the lamina [Laughlin, 1994; James, 1990]. Recordings and modelling by James (1990) from the temporal impulse responses of LMCs (in the hover fly *Eristalis*), reveals that the LMCs have the characteristic of the difference of two log-normal functions. Addition of this temporal band pass filter is found to increase the peak response velocity and reduce the variance of the correlator output [Dror, 1998].

Hence in our experiments, the image in Figure 3 is temporally filtered with a difference of log-normal filter to copy the response of the lamina monopolar cells [James, 1990; Payne and Howard, 1981; Howard et al., 1984].

8.2.3 Output Integration

Integration in space or time has been extensively used to produce reliable motion signals [Reichardt, 1961; van Santen and Sperling, 1985a; Borst and Egelhaaf, 1989; Hausen and Egelhaaf, 1989; Borst and Egelhaaf, 1994]. Integration involves a tradeoff between accuracy of velocity estimation and resolution in space and time. In insects, the lobula which contains wide field directionally selective motion detection neurons are responsible for the detection of whole field or whole frame motion. In the lobula, the output of the local retinotopic movement detectors is pooled. This is accomplished in the dendrites of the tangential cells in the lobula plate [Hausen and Egelhaaf, 1989]. Intracellular recordings from the wide field cells indicate that they sum the outputs of local Reichardt correlators in their receptive fields [Egelhaaf et al., 1989]. Integration is found to lower the relative error by decreasing the variance of the output signal. It is seen that the decrease is more significant in the presence of saturation [Dror, 1998]. Our EMD array model copies the lobula by averaging the outputs to produce an average EMD response.

8.3 Elaborated EMD model with adaptation

In our elaborated Reichardt correlator array model, in order to reduce the dependency of the response to changes in contrast and spatial frequency and to get a more accurate estimate of velocity, contrast gain reduction is implemented as a dynamic non-linearity in which the EMD output is fed back to control the input gain as in Figure 5.7 in Chapter 5.

In order to understand the performance of the model with and without adaptation, we calculate the simulated relative error of the adapted and non-adapted elaborated EMD model. The simulated relative error of the adaptive EMD array model is then compared to that of the non adaptive-elaborated EMD array model. Figure 8.2 shows the relative error of one row of the EMD array of the elaborated EMD model with adaptation compared to that of the elaborated EMD model without adaptation. It is seen that even though adaptation reduces the dependence of the response to contrast, it increases the relative error and the relative error increases with increase in the velocity because adaptation introduces more variation in the correlator response and hence more errors at higher velocities.

Figure 8.3 shows the simulated mean relative error of total elaborated EMD array with adaptation with the response averaged over 4 images, at 5 different speeds. It is seen that averaging of all the rows of EMDs (spatial integration at the output) reduces the relative error that is shown Figure 8.2, where only one row of EMDs are taken. It is seen that even though adaptation reduces the dependence of the response to contrast, it increases the relative error and the relative error increases with increase in the velocity because adaptation introduces more variation in the correlator response and hence more errors at higher velocities. It is also seen from both the figures that output integration or averaging of all the rows of EMDs reduces the relative error seen in Figure 8.2.

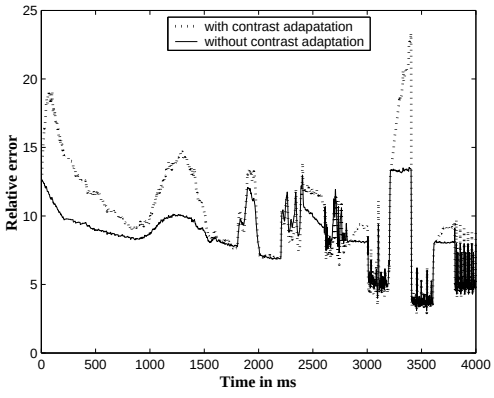

Fig. 8.2. Comparison of simulated relative error with contrast adaptation and without contrast adaptation. The simulated relative error of one row of the EMD array of the elaborated EMD model with adaptation is compared to that of the elaborated EMD model without adaptation. It is seen that even though adaptation reduces the dependence of the response to contrast, it increases the relative error.

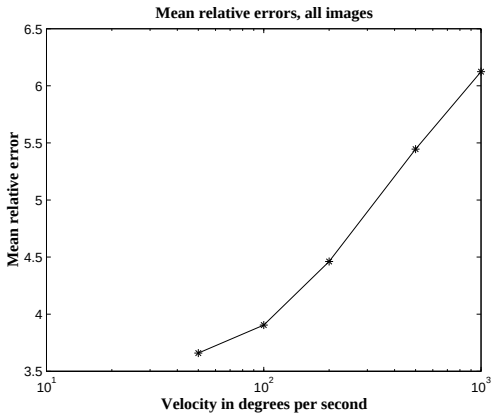

Fig. 8.3. Simulated mean relative error of our elaborated EMD model. This figure shows the simulated mean relative error of total elaborated EMD array model including feedback adaptation with the response averaged over 4 images shown in Figure 8.1, at 5 different speeds. It is seen that averaging of all the rows of EMDs (spatial integration at the output) reduces the relative error that is shown Figure 8.2, where only one row of EMDs are taken. It is seen that even though adaptation reduces the dependence of the response to contrast, it increases the relative error and the relative error increases with increase in the velocity because adaptation introduces more variation in the correlator response and hence more errors at higher velocities.

8.3.1 Saturation

Next saturation is added in the model and the performance of the model with saturation added at different position is tested in terms of relative error.

8.3.2 Saturation at the correlator input

Saturation of the visual signal first occurs in the photoreceptors, which respond roughly to logarithm of luminance [Laughlin, 1994]. Saturation reduces relative error partly by reducing contrast difference from one region of the image to another. It is seen in flies that this saturation occurs primarily after linear pre-filtering but before the multiplication operation indicating that contrast saturation must take place after elimination of the mean light intensity from the signal [Egelhaaf et al., 1989; Allik and Pulver, 1995; Dror, 1998]. Saturation is modelled here by including a compressive non-linearity such as a hyperbolic tangent function of the form, $\rho(C) = \tanh(C)$.

In the model, saturation is implemented on the spatially pre-filtered input. The effect of this saturation and adaptation on the model is shown in the Figure 8.4 and Figure 8.5.

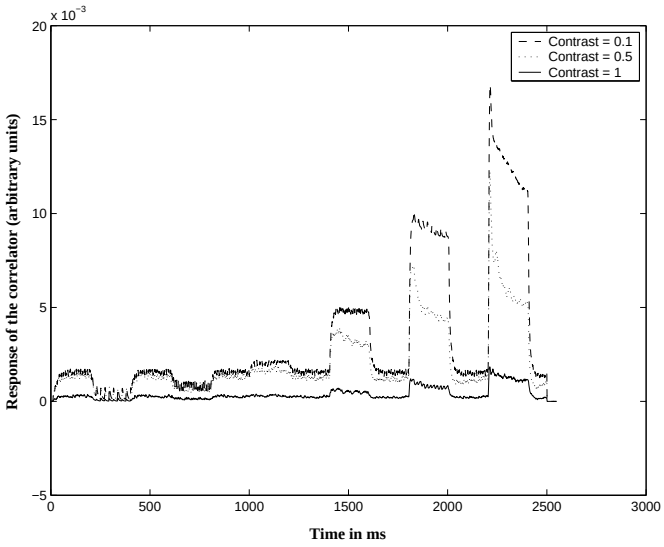

Figure 8.4. Simulated mean correlator response with saturation implemented at the photoreceptors at three different contrasts. The simulated mean correlator response of one row of EMDs for three different contrast (1, 0.5 and 0.1) including saturation at the photoreceptors and feedback contrast adaptation is shown here. It is seen that due to the saturation effects, the correlator response is squashed and the response increases at low contrasts. It is also seen that the dependence of the response on contrast is further reduced by adding input saturation along with adaptation.

Figure 8.4 shows the mean response of one row of EMDs for three different contrasts (1, 0.5 and 0.1) including saturation at the photoreceptors and feedback contrast adaptation. The simulation is performed on one image, image 1 shown in Figure 8.1, moving at low adapting speed of 5 degrees per second. The saturation compresses the correlator response and the effect of saturation causes the response to increase with decrease in contrast. It is also seen that the addition of input saturation to adaptation further reduces the dependence of the response to contrast.

Figure 8.5 shows and the simulated mean relative error of the elaborated EMD model with input saturation and adaptation obtained by testing the model over 4 different images given in Figure 8.1. It is seen that the relative error is greatly reduced by the addition of saturation (compressive nonlinearity) at the input along with adaptation.

8.3.3 Saturation at the correlator arms

It is also seen that saturation also takes place on both the delayed and un-delayed arms of the correlator with saturation on the delayed arm following the delay filter [Egelhaaf et

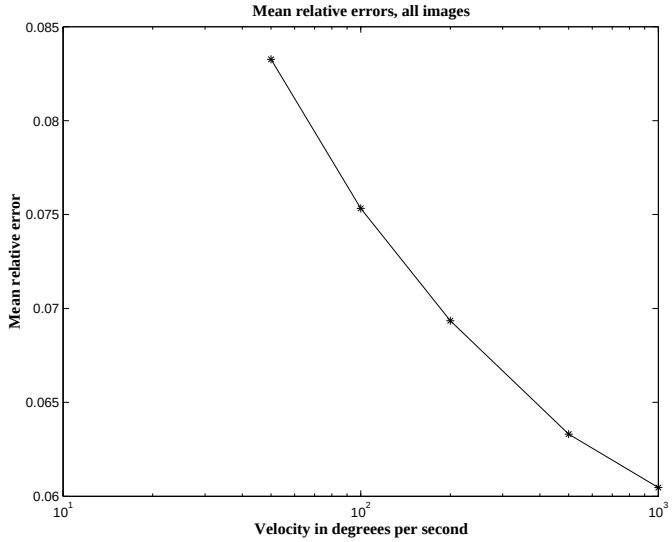

Fig. 8.5. Simulated mean relative error of the elaborated EMD model with adaptation and saturation at the input. This figure shows the simulated mean relative error of the elaborated EMD array model including feedback adaptation and input saturation with the response averaged over 4 images, at 5 different speeds. The relative error is greatly reduced by the addition of saturation (compressive nonlinearity) at the input along with adaptation.

al., 1989; Dror, 1998]. So based on this, compressive nonlinearity is implemented before the multiplication operation on both correlator arms.

Figure 8.6 shows the simulated mean corrlator response of one row of EMDs for three different contrast (1, 0.5 and 0.1) including saturation at the correlator arms, saturation at the photoreceptors and feedback contrast adaptation. As expected, due to the saturation effects, the response is higher at lower contrasts and the dependance of the response on contrast is further reduced. The correlator response is further squashed due to the additional compressive non linearity added. Figure 8.7 compares the simulated mean response of one row of EMDs of an elaborated model with feedback adaptation and saturation at the photoreceptors with that of the elaborated model including feedback adaptation, saturation at the input and saturation at both the correlator arms. The addition of compressive non-linearity further squashes the response of the correlator.

8.4 EMD model with adaptation and saturation

Figure 8.8 shows the block diagram of an elaborated EMD model with adaptation and saturation. The saturation or compressive-nonlinearity is implemented on the spatially

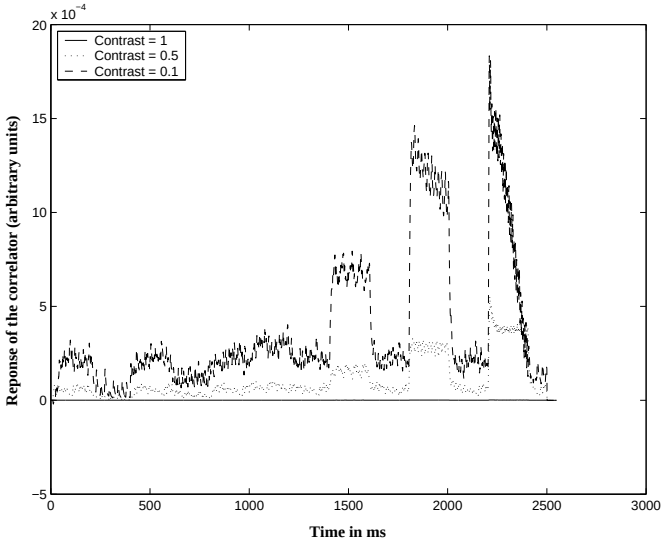

Figure 8.6. Simulated mean correlator response at three different contrast with saturation implemented at the input and arms. The simulated mean corrlator response of one row of EMDs for three different contrast (1, 0.5 and 0.1) including saturation at the correlator arms, saturation at the photoreceptors and feedback contrast adaptation is shown here. Due to the saturation effects, the response is higher at lower contrasts and the dependance of the response on contrast is further reduced. The correlator response is further squashed due to the additional compressive non-linearity.

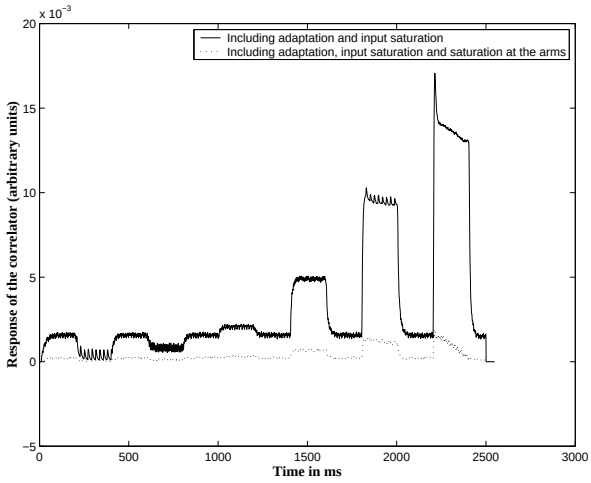

Figure 8.7. Comparison of simulated mean correlator response with saturation included at the input with that of the model with saturation implemented at the input and arms. This figure compares the simulated mean response of one row of EMDs of an elaborated model (at contrast = 0.1) with feedback adaptation and saturation at the photoreceptors with that of the elaborated model including feedback adaptation, saturation at the input and saturation at both the correlator arms. It is seen that the addition of compressive non-linearity further squashes the response of the correlator.

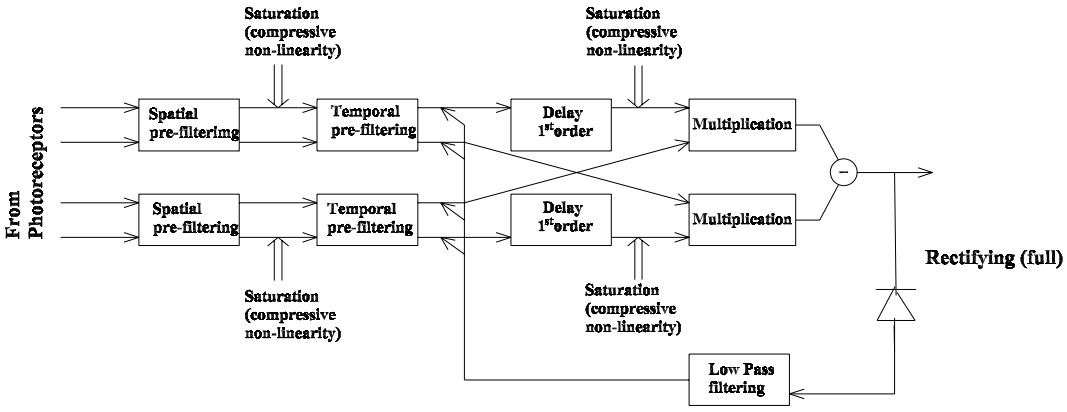

Figure 8.8. Block diagram of an elaborated EMD model including feedback adaptation and saturation. The saturation or compressive-nonlinearity is implemented on the spatially filtered input and at the correlator arms. The rectified and low pass filtered output is fed back to control the gain of the input in this feed back adaptive model.

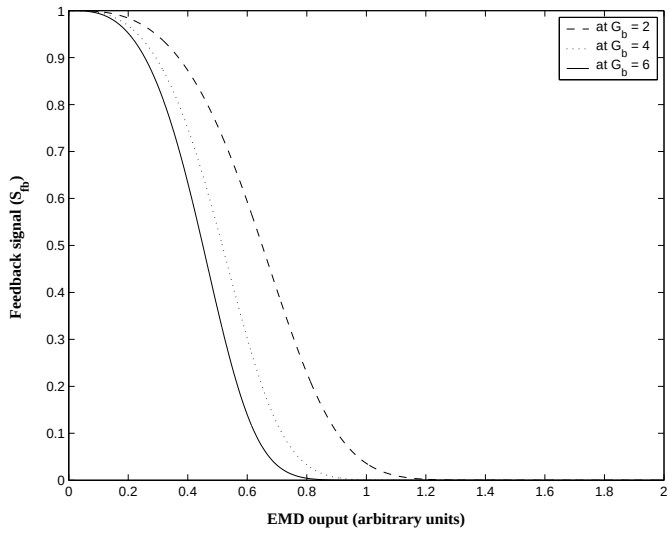

Figure 8.9. The variation of feedback signal (S_{fb}) as the correlator output is increased is shown here. It is seen clearly at very low response, our elaborated model behaves like a simple correlator. But as the correlator response increases the feedback signal decreases and then eventually becomes zero at high EMD outputs. The response of the feedback signal at three values of G_b (2,4 and 6) are shown here. As the feedback gain increases, the curve shifts to the left and the starts becoming more linear and the response of the feedback signal falls to zero at lower values.

filtered input and at the correlator arms. The rectified and low pass filtered output is fed back to control the gain of the input in this feed back adaptive model.

The feedback signal fed to the correlator arms is given by

$S_{\text{fb}} = 1 - \tanh(G_{\text{b}} \times \text{EMD}_{\text{out}}^3)$

Where EMD_{out} is the rectified and low pass filtered output of the EMD and G_{b} is a constant which is the feedback gain.

The variation of the feedback signal as the feedback gain is increased is shown in Figure 8.9. It is seen clearly that at very low response, our elaborated model behaves like a simple correlator. But as the correlator response increases the feedback signal decreases and then eventually becomes zero at high EMD outputs. The response of the feedback signal at three values of G_b (2,4 and 6) are also shown. As the feedback gain increases, the curve shifts to the left and starts becoming more linear and the response of the feedback signal falls to zero at lower values.

Figure 8.10 shows the simulated mean relative error of the elaborated EMD model with all elaborations obtained by testing the model over 4 different images given in Figure 8.1. It is seen that the relative error goes slightly higher by adding the saturation at the correlator arms along with input saturation. Relative error with only the input saturation is very low. But when saturation at the arms is added, the relative error rises slightly but is still very low compared to the relative error without any saturation and only with adaptation shown in Figure 8.2. Hence even though saturation at the arms along with input saturation increases relative error slightly it further decreases the dependance of the response to contrast as is seen in Figure 8.6.

Hence from all these figures it is seen that the addition of the various elaborations to the Reichardt correlator decreases the dependence of the response to contrast and lowers the relative error [Rajesh et al., 2004].

8.4.1 Coefficient of Variation

In order to further demonstrate the improvement in the model with the inclusion of non-linearities like adaptation and saturation, we conducted a test adapt test experiment where we used a large set of 18 natural panoramic images shown in [Brinkworth and O'Carroll, 2007] running at the same test speed and adapting speed. In order to account for all types of stimuli, we have also included stimuli which are deliberately sparse that

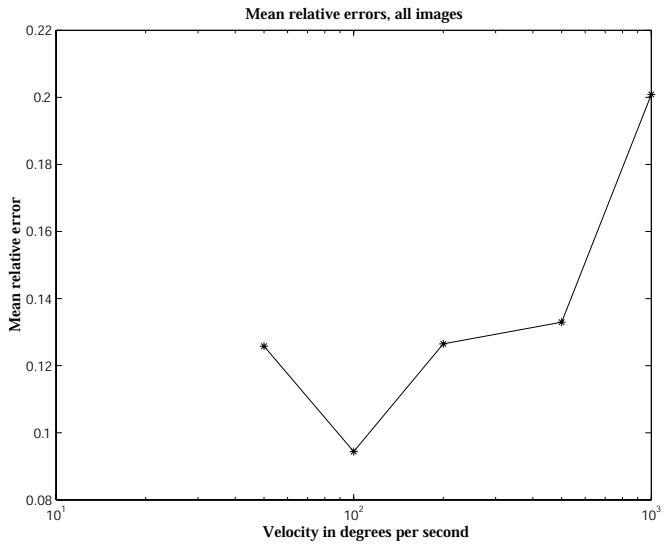

Fig. 8.10. Simulated mean relative error of the total elaborated model. This figure shows the simulated mean relative error of total elaborated EMD array model including feedback adaptation, input saturation and saturation at the correlator arms with the response averaged over 4 images, at 5 different speeds.

we know would drive very weak signals to compare their performance with other natural image stimuli. These images are all run through our elaborated model with feedback adaptation and saturation at the input,arms and output, at the same test speed of 45°/s and an adapting speed of 200°/s.

The addition of the feed back adaptation results in increase in adaptation for higher contrasts images there by decreases their responses. Similarly due to the presence of feedback adaptation, there is very little adaptation seen taking place here for the low contrast images as can be noted in Figure 8.11. Hence it can be seen that the implementation of feedback adaptation hence helps to decrease the contrast variation in the natural images there by improving the velocity performance of the model. The presence of saturation compresses the response at higher contrasts to further improve the velocity constancy of the response.

Figure 8.12 shows the overall mean value before and after adaptation with error bars. The result of the post adaptation stage shows a decrease in the error thereby improving model output.

The coefficient of variation (CV) is then calculated for the response before adaptation and after adaptation to understand the effect of adaptation and saturation in the model. The coefficient of variation is a normalized measure of dispersion of a probability distribution.

It is defined as the ratio of the standard deviation to the mean. It gives the value of variability of the response between different animated scenes of the model before and after adaptation [Shoemaker et al., 2005]. The coefficient of variation for this experiment shown in Figure 8.13 demonstrates improvement with the inclusion of additional non-linearities. The responses shown at the bottom of the figures are the responses of the outlier images with weak contrast features that were deliberately included in our image set. As expected the responses of these outlier images are weak compared to responses of other images. The performance of the model could be further enhanced at the post adaptation stage by further increasing the output saturation which could be explored in future experiments.

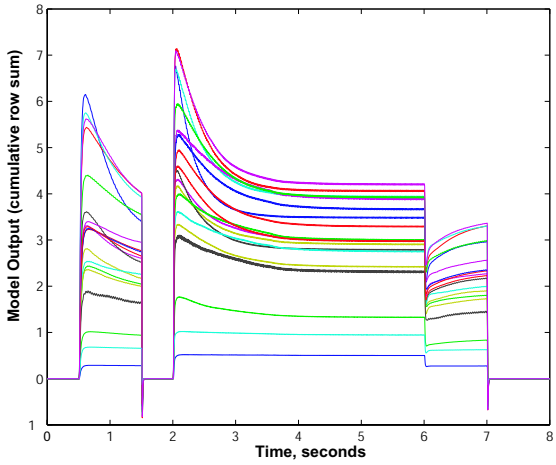

Fig. 8.11. Simulated cumulative sum of mean correlator responses of the total elaborated model for a large set of images.. This figure shows the simulated cumulative sum the mean response of total elaborated EMD array model including feedback adaptation, and saturation for 18 images shown in [Brinkworth and O'Carroll, 2007], all running at the same single test speed of $45°/s$ and an adapting speed of $200°/s$.

8.5 Conclusion

The main idea of this study is to develop an elaborated EMD array model capable of accurate velocity estimation. In this chapter, a comparative study on the effect of each of the elaboration on the performance of our model is carried out. Relative error and coefficient of variation are calculated to understand the performance of the model with and without additional non-linearities. Relative error experiments shows that the addition of adaptation reduces relative error. But there is a significant reduction of relative error with

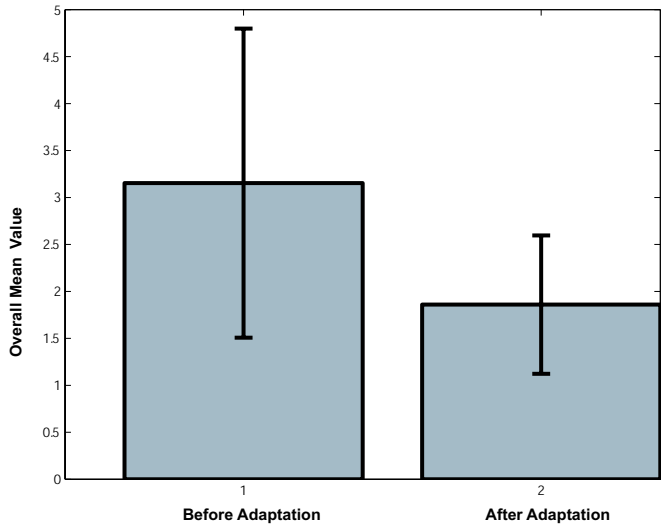

Fig. 8.12. The bar graph showing the mean response with error bars before the adaptation stage and after adaptation.. This figure shows the bar graph of overall mean of the correlator response with error bars of total elaborated EMD array model including feedback adaptation and saturation for 18 images, all running at the same single test speed of $45°/s$ and an adapting speed of $200°/s$.

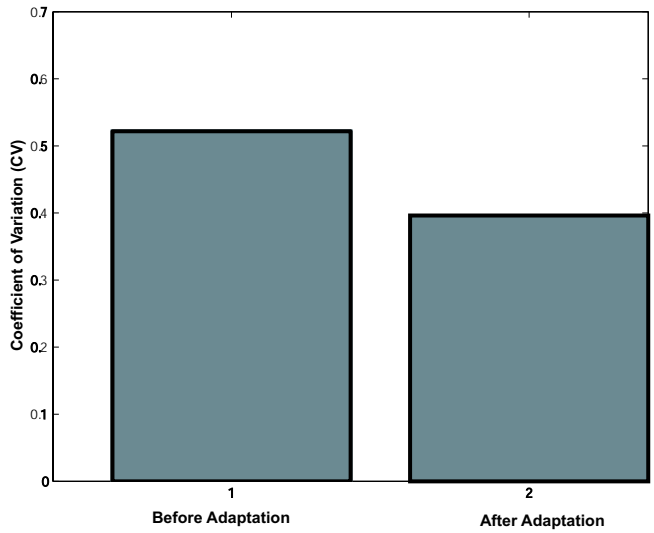

Fig. 8.13. The bar graph showing the coefficient of variation before adaptation and after adaptation of the elaborated model. This figure shows the simulated mean relative error of total elaborated EMD array model including feedback adaptation and saturation for 18 images, all running at the same single test speed of $45°/s$ and an adapting speed of $200°/s$. The improvement in performance of the model after adaptation is indicated by the reduction in the coefficient of variation shown here.

the addition of saturation and the improvement in velocity performance with the inclusion of saturation is also shown. The test adapt test experiment compares the coefficient of variation between the responses before and after the adaptation stage. It is seen that there is reduction in coefficient of variation after the adaptation stage suggesting improvement in the performance of the model with the inclusion of additional non-linearities.

The comparative study of the influence of the elaborations and the study of the relative error provides us with an insight on how to further improve the model, based on the physiological knowledge of the fly visual system. Further physiological experiments are carried out to explore the performance of the model and a comparative study on the performance of our model with the physiological experiments carried out on insect neurons using the same stimuli is shown in the next chapter.

Chapter 9

Pattern noise study on different image structures

IN this chapter, the response of the elaborated model is compared with the fly HS neuron response to naturalistic image panoramas. This response is dominated by noise which is largely non-random. To investigate the influence of anisotropic features in producing pattern noise, several panoramic images are presented at various initial positions, and versions of the same images are modified to disrupt vertical contours. These images are then presented at a range of speeds that are relevant to the species studied. It is seen that the response of the fly neurons shows evidence of local saturation at key stages in the motion pathway. This saturation is found to reduce the effect of pattern noise and to improve the coding of velocity. This model hence provides an excellent basis for the development of biomimetic yaw sensors for robotic applications.

9.1 Response of Fly HS Neurons to Naturalistic Images

Natural images are far from random and show a large degree of structure. This structure can be described by the statistics of the image source, and can be considered as prior knowledge. Therefore a certain amount of image data is predictable and thus redundant [Ruderman, 1994; van der Schaaf and van Hateren, 1996]. The visual system appears to be optimized to take advantage of the statistical properties of natural images using specific optimization criteria of redundancy minimization, maximisation of information transmission, sparseness of the neural coding and minimising reconstruction error, demonstrating that simple optimisation principles combined with knowledge of image statistics can predict visual processing strategies that are found in nature [Ruderman, 1997]. In insect vision, outputs of local motion detectors are collated by a system of tangential neurons tuned to very specific types of complex motion. Differences in the local structure of natural images result in variations in the correlator response of the local detectors, which is termed as *pattern noise*.

Among the best studied LPTCs in the blowfly are the large, graded neurons forming the so called vertical system ('VS') and horizontal system ('HS'). The HS system contains three neurons in each hemisphere, that view the dorsal (HSN—north), medial (HSE—equatorial) and ventral (HSS—south) visual field respectively [Hausen, 1982c]. The receptive field properties led to the proposal that HS cells were matched filters primarily concerned with detection of rotational motion about the yaw axis [Krapp et al., 1998; Krapp et al., 2001]. Arguing against the matched filter hypothesis, however it is recently shown that HS cells may also respond strongly during translation [Karmeier et al., 2006; Kern et al., 2005]. But recent findings by Nordstorm et al. (2007) show that the physiological properties of one of these neurons (HSN) are strongly in support of a role in yaw rotation detection either during hovering or rapid forward flight, and are inconsistent with a likely role in forward translation thus supporting the matched filter hypothesis for optic flow analysis.

9.1.1 Evidence of Pattern Noise—Electrophysiology Results

Naturalistic panoramic images shown in Figure 9.1 were displayed on the inside of a virtual cylinder, which was centered on the fly (*Eristalis tenax*, male) and perspective distorted according to the fly's calibrated 3D position and orientation relative to the CRT. Motion simulated pure yaw rotations by spinning the virtual cylinder about a dorsal-ventral axis

Figure 9.1. The panoramic natural images given as stimulus to the EMD model. A panorama of the image is formed by 'warping' 12 image tiles at 30° intervals to remove lens distortions and then by wrapping its ends together using Apple Quicktime VR software on a Macintosh computer.

of the fly's head. The display subtended approximately 90 degrees horizontally from the midline to the lateral portion of the animal, thus stimulating most of the receptive field of the HS neurons (See Figure 9.2).

In the present study we chose three naturalistic images that differ in aggregated natural contrast $\bar{C}_n$ approximately by a factor three. In the first set of experiments the three selected images were presented to the insect at a constant speed of 180°/s, which is a value close to the optimal velocity in *Eristalis tenax*. A particular image was presented in eight trials. The stimulus period was long enough for the image to pass the HS cell's receptive field twice completely.

From one trial to the next the image's starting position was shifted by 45 degrees, i.e. in the stimulus periods of the seven trials following the first trial the stimulus was phase-shifted by 45, 90, 135, ...,315 degrees. Figure 9.3 shows the HS cell's response to such a sequence of naturalistic stimuli at various phase shifts.

The response functions that make up a set of eight trials were aggregated in two different ways. The first is 'time-aligned' response where the response is aligned by stimulus time. Because the initial phase is different in each trial, phase dependent noise (pattern noise)

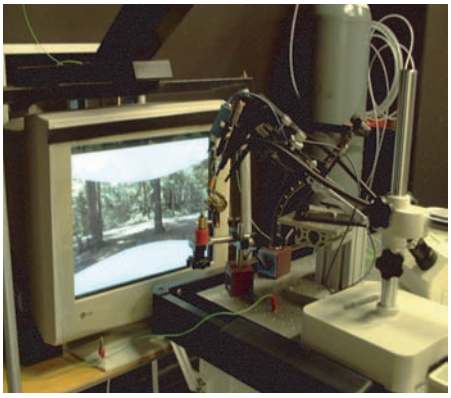

Figure 9.2. Electrophysiological experimental set up. Male hoverflies (*Eristalis tenax*) were positioned upright on a stand, which was mounted on a Newport anti-vibration recording table with a stimulus monitor in front of the fly. Naturalistic panoramic images were displayed on the inside of a virtual cylinder, which was centered on the fly and the perspective distorted according to the fly's calibrated 3D position and orientation relative to the screen. Motion simulated pure yaw rotations by spinning the virtual cylinder about a dorsal-ventral axis of the flies head. The display subtended approximately 90 degrees horizontally from the midline to the lateral portion of the animal, thus stimulating most of the receptive field of HS neuron.

disappears in the average, just as if we had simulated a 360 degree EMD array. The second is 'phase-aligned', where we align each phase-delayed image with the data obtained for phase zero, so that it is the image position that is averaged, rather than time. Averaging in these two different ways produces different results.

Figure 9.3 shows the comparison of physiological and modelling results using the same stimulus at different phases and their phase aligned and time aligned responses. On the left hand side, this figure shows the response of the HS neuron to Image 1, with the image presented moving at 180°/s at 8 different initial phases, each 45 degrees apart. Graph (a)shows the response to each of these 8 configurations. Graph (b) shows the response averaged in two ways, time aligned and phase aligned. In the time aligned method, the normal average of the each of the eight response removes the pattern noise as the response is aligned by stimulus time. In the phase aligned method, each phase delayed image is aligned with the data obtained for phase zero and then it is averaged. Now the pattern noise is still present because in this way, it is the image position that is averaged rather than time, and it can be still seen as the noise is locked in the stimulus position. On the right hand side, this figure shows the modelling results for the same experiment with the same Image 1 using our elaborated Reichardt model. Graph (c) shows the response of

our model at 8 different initial positions and part (d) shows the time aligned and phase aligned graphs obtained with our model. The phase aligned graph from the model differs in shape with pattern noise shape seen in the response of the HS neuron here. This could be because saturation is not included here in this model at this point.

By comparing the relative error of the time aligned responses to that of the phase aligned responses in Figure 9.3, we can see the 'pattern noise' dominating the phase-aligned response, indicating the impact of spatial structure in naturalistic stimuli on HS cells response to constant velocity.

9.1.2 Evidence of Pattern Noise—Modelling Results

The same experiments are repeated with the elaborated model using the same stimuli shown in Figure 9.1 at the same speed of 180°/s. Then the time aligned and the phase aligned response are created, as before, using the elaborated Reichardt model. By aligning response curves in time across several initial positions, pattern noise is largely removed from the mean, but contributes significantly to the standard deviation as can be seen by aligning response curves by position.

Comparing the phase aligned response of the model with the physiological data in Figure 9.3, it is seen that the shape of pattern noise differs in the model from that of the response of the HS neuron. This could be because this model has no compressive non-linearity implemented in it. So the experiment is repeated with saturation added to the model at different positions and the effect of saturation on pattern noise is studied in the next section.

9.2 Implementation of Saturation

Both simple and elaborated Reichardt correlators show an increase of response amplitude with stimulus contrast. The neural and behavioral responses of the fly display such a dependence only at very low contrasts. As contrast increases above a few percent, the response begins to level off due to a static, compressive non-linearity, which is termed *contrast saturation* [Dror, 1998]. This is due to limitations in the range of responses that can be signaled by physiological mechanisms.

Saturation of the visual signal first occurs in the photoreceptors, which respond roughly to logarithm of luminance [Laughlin, 1994]. Saturation reduces relative error partly by

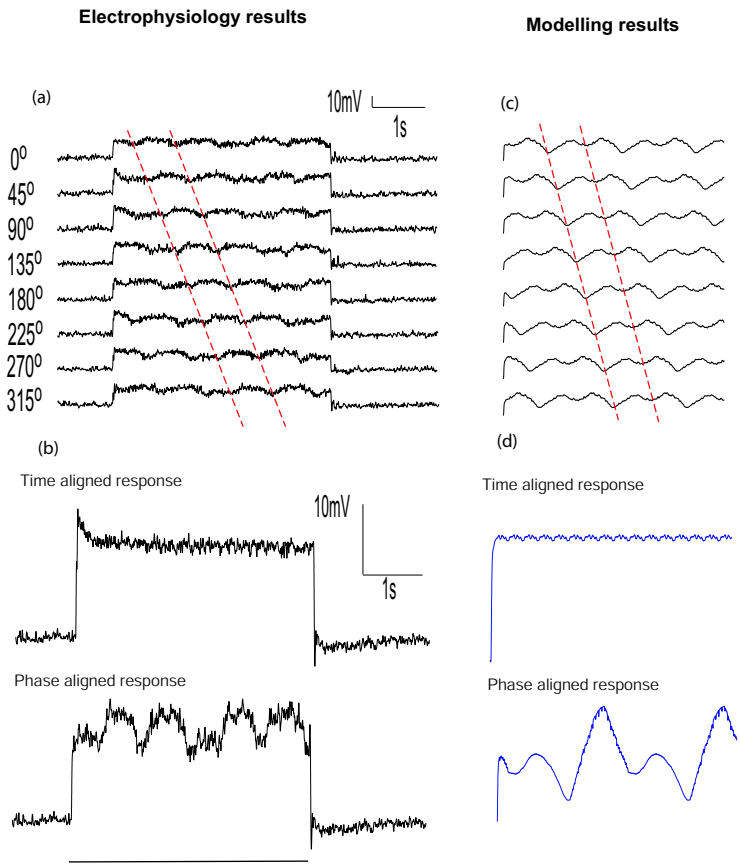

Figure 9.3. Comparison of physiological and modelling results using the same stimulus at different phases and their phase aligned and time aligned responses. On the left hand side, this figure shows the response of the HS neuron to Image 1, with the image presented moving at $180°/s$ at 8 different initial phases, each 45 degrees apart. Graph (a)shows the response to each of these 8 configurations. Graph (b) shows the response averaged in two ways, time aligned and phase aligned. In the time aligned method, the normal average of the each of the eight response removes the pattern noise as the response is aligned by stimulus time. In the phase aligned method, each phase delayed image is aligned with the data obtained for phase zero and then it is averaged. Now the pattern noise is still present because in this way, it is the image position that is averaged rather than time, and it can be still seen as the noise is locked in the stimulus position. On the right hand side, this figure shows the modelling results for the same experiment with the same Image 1 using our elaborated Reichardt model. Graph (c) shows the response of our model at 8 different initial positions and part (d) shows the time aligned and phase aligned graphs obtained with our model. The phase aligned graph from the model differs in shape with pattern noise shape seen in the response of the HS neuron here. This could be because saturation is not included here in this model at this point.

reducing contrast difference from one region of the image to another. It is seen in flies that this saturation occurs primarily after linear pre-filtering, but before the multiplication operation indicating that contrast saturation must take place after elimination of the mean light intensity from the signal [Egelhaaf et al., 1989; Dror, 1998]. Saturation is modelled here by including a compressive non-linearity such as a hyperbolic tangent function of the form, $\rho(C) = \tanh(C)$.

It is also seen that saturation also takes place on both the delayed and un-delayed arms of the correlator with saturation on the delayed arm following the delay filter [Egelhaaf et al., 1989; Dror, 1998]. So based on this, compressive nonlinearity is implemented before the multiplication operation on both correlator arms.

The outputs of the wide field neurons are also found to saturate due to shunting of the membrane potential [Single and Borst, 1998]. This is introduced as a compressive non-linearity following spatial integration [Dror, 1998]. Such an effect will flatten the peaks of the velocity response curves effectively allowing neuron to use more of its dynamic range to signal low velocities. So based on this, saturation is implemented also at the output stage of our model.

A significant effect on the shape of pattern noise is seen when saturation is added at various locations within the model. Here the modelling results are explored with saturation at the photoreceptors (input), at the correlator arms and at the output after spatial integration of the correlator outputs as shown in Figure 9.4. In this figure, phase aligned simulation results obtained by running the model at 180°/s using the image 1 shown in Figure 9.1 at a contrast of 1 are shown. Saturation is implemented at the input stage, at the photoreceptors, at the correlator arms before multiplication and on the mean correlator output individually and also combination of saturation at different places and the phase aligned responses showing the pattern noise in each case is shown here. Note that each combination of saturation implemented at different positions have a significant effect on the shape of the pattern noise indicating that perhaps saturation has a key role in influencing pattern noise in the fly motion pathway.

Figure 9.5 shows the phase aligned simulation results obtained from the elaborated model with the combination of saturation implemented at the correlator arms and at the output, superimposed on the physiological data. Initial results show that saturation implemented at the correlator arms and at the mean correlator output seemed to produce the most closest match with the physiological data. But more proper scaling and calculation of the cross-covariance discussed further in this Chapter does not agree with this conclusion.

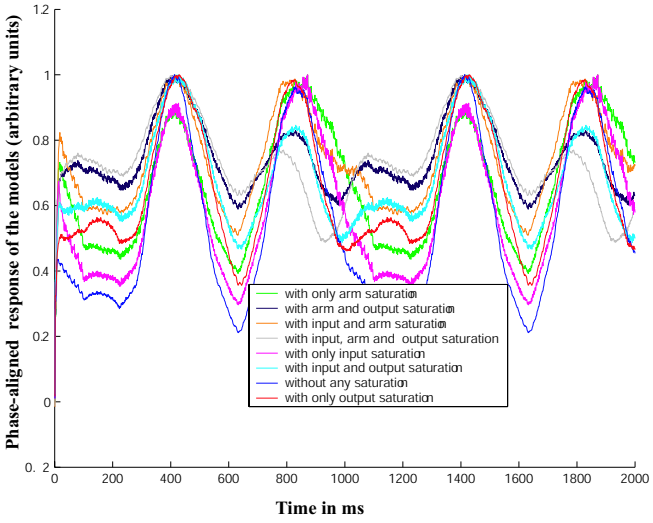

Figure 9.4. Phase aligned simulation results obtained by running the model at $180°/s$ using the image 1 shown in Figure 9.1 at a contrast of 1. Saturation is implemented at the input stage, at the photoreceptors, at the correlator arms before multiplication and on the mean correlator output individually and also combination of saturation at different places and the phase aligned responses showing the pattern noise in each case is shown here. Note that the saturation implemented at different positions have a significant effect on the shape of the pattern noise indicating that perhaps saturation has a key role in influencing pattern noise in the fly motion pathway.

9.3 Images with Disrupted Vertical Contours

Since pattern noise responds to the structural features of the images and in this case because the model is looking at horizontally selective EMDs, mainly vertical contours, versions of the image shown in Figure 9.1,is changed so that these images have disrupted vertical contours and these disrupted images are then used as stimuli. For this, each image is split into four equal parts horizontally. Then the first part is shifted 90 degrees, the second part is shifted 180 degrees, the third portion 270 degrees and the fourth part 360 degrees so as to completely disrupt their vertical contours. Then these disrupted images are used as stimuli to study pattern noise.

Figure 9.7 shows the phase aligned simulation results obtained by running the model at $180°/s$ using the disrupted Image 1 shown in Figure 9.6 at a contrast of 1. Saturation is implemented at the input stage, at the photoreceptors, at the correlator arms before multiplication and on the mean correlator output individually and also combination of

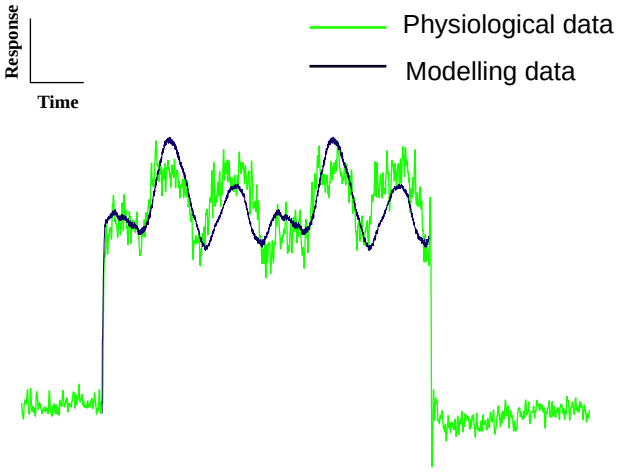

Figure 9.5. Phase aligned simulation results obtained from the elaborated model with saturation implemented at the correlator arms and at the output, superimposed on the physiological data. Both the physiology and modelling experiments are performed using Image 1 moving at a speed of 180°/s at a contrast of 1. In the phase aligned method, each phase delayed responses aligned by shifting each response along the x-axis with the data obtained for phase zero and then it is averaged.

saturation at different places are also used and the phase aligned responses showing the pattern noise in each case is shown here. Here also noted that the saturation implemented at different positions have a significant effect on the shape of the pattern noise indicating that perhaps saturation has a key role in influencing pattern noise in the fly motion pathway. Figure 9.8 shows the phase aligned simulation results obtained from the elaborated model with saturation implemented at the correlator arms and at the output, superimposed on the physiological data. Initial results with disrupted images show that saturation implemented at the correlator arms and at the mean correlator output seemed to produce the most closest match with the physiological data. But more proper scaling and calculation of the cross-covariance discussed further in this Chapter does not agree with this conclusion.

Figure 9.9 shows the response of three HS cells to the three images of Figure 9.1 and their shifted versions (shown in Figure 9.6). In this figure it is noted that pattern noise occurs for all images and that it is specific for each image. Comparing the original images with its modified versions, it can be seen that the pattern noise has changed. Peaks are found to be typically reduced and often phase-shifted. Presenting a range of different images shows not only that pattern noise occurs in many naturalistic images but also that the actual deviations are quite different in the responses to different images. It is as if the

Image 1

Image 2

Image 3

Figure 9.6. The three images of Figure 9.1 with their vertical contours disrupted.. For this, each image is split into four equal parts horizontally. Then the first part is shifted 90 degrees, the second part is shifted 180 degrees, the third portion 270 degrees and the fourth part 360 degrees so as to completely disrupt their vertical contours. Then these disrupted images are used as stimuli to study pattern noise.

pattern noise component is a 'finger print' of the spatial image spectra. Figure 9.10 shows the modelling results obtained for the three images and their disrupted counterparts. in this figure also it can be seen that pattern noise occurs for all images and it is different for different images. Comparing the original image with its modified versions in the modelling data, it can be seen that like in the physiological data, the pattern noise has changed and the shifted counterparts show phase-shifts in their response. It is seen that the modelling results also reveal that the different pattern noise for different images show that they are dependent on the spatial content of the natural scene [Rajesh et al., 2005b].

There are also considerable differences in the pattern noise component of the responses to the shifted and unshifted images. Figure 9.9 and Figure 9.10 (both physiology and modelling results) shows that while much of the shapes of the pattern noise is preserved between images, there are some amplitude changes and phase shift in the response of the

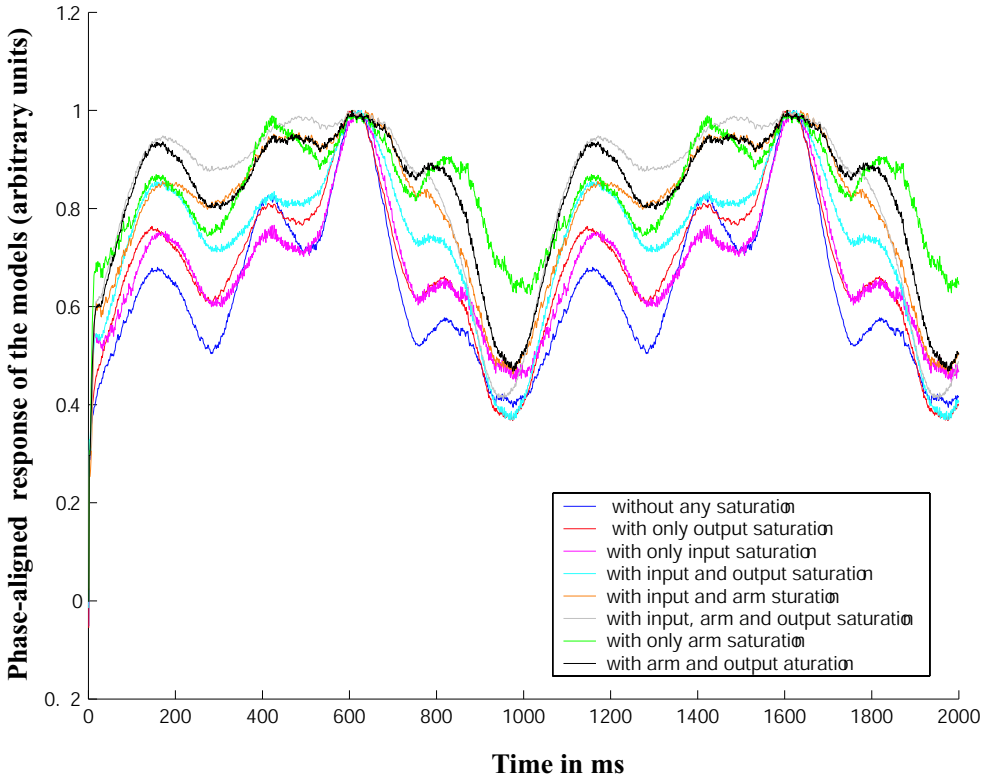

Figure 9.7. Phase aligned simulation results obtained by running the model at 180 degrees per sec using the disrupted image 1. This figure shows the phase aligned simulation results obtained by running the model at 180 degrees per sec using the disrupted Image 1 shown in Figure 9.6 at a contrast of 1. Saturation is implemented at the input stage, at the photoreceptors, at the correlator arms before multiplication and on the mean correlator output individually and also combination of saturation at different places is also used and the phase aligned responses showing the pattern noise in each case is shown here. Note that the saturation implemented at different positions have a significant effect on the shape of the pattern noise indicating that perhaps saturation has a key role in influencing pattern noise in the fly motion pathway.

disrupted images. All these results strongly reiterates that pattern noise depends on the structural nature of the stimulus.

9.4 Pattern Noise Analysis Using Different Images

In order to gain a better understanding of the affect of saturation on pattern noise, the influence of saturation implemented at different positions of the model in different images is studied.

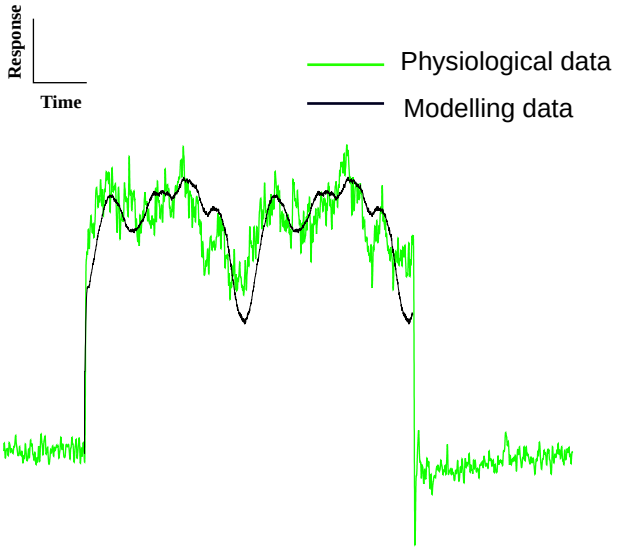

Figure 9.8. Phase aligned simulation results obtained from the elaborated model with saturation implemented at the correlator arms and at the output, superimposed on the physiological data using disrupted image 1. Both the physiology and modelling experiments are performed using Image 1 moving at a speed of 180 degrees per sec at a contrast of 1. In the phase aligned method, each phase delayed response is aligned by shifting each response along the x-axis with the data obtained for phase zero and then it is averaged.

In all the eight cases the phase aligned data, which shows the maximum pattern noise, is compared to the phase aligned physiological data. In order to evaluate and compare each of the modelled response with the fly's response, the cross covariance value is calculated.

The experiment is repeated using the three different images seen in Figure 9.1 at the optimum speed of 180°/s and at a maximum contrast of 1. The results obtained in each case are shown in the Figures 9.11, 9.12 and 9.13 and the cross covariance values and the relative error values calculated for each case are shown in the Table 1and Table 2 9.4. Cross covariance is a measure of similarity of two signals. True cross covariance is the cross-correlation of mean-removed sequences. Since comparison is conducted on the shape of the two signals, the DC value is of no interest and it is subtracted before cross correlation is performed. This results in cross covariance measure which is used here to compare the physiology and modelling response.

The error measure used here called the relative error defined by Dror as, $E_{\text{rel}} = E_{\text{abs}}/\overline{R}$, where the absolute error (E_{abs}) is the difference between the actual response and the expected response [Dror, 1998]. The expected response is the mean response value that is given by $\overline{R}$. For a given set of images, moving at a given velocity, the mean response

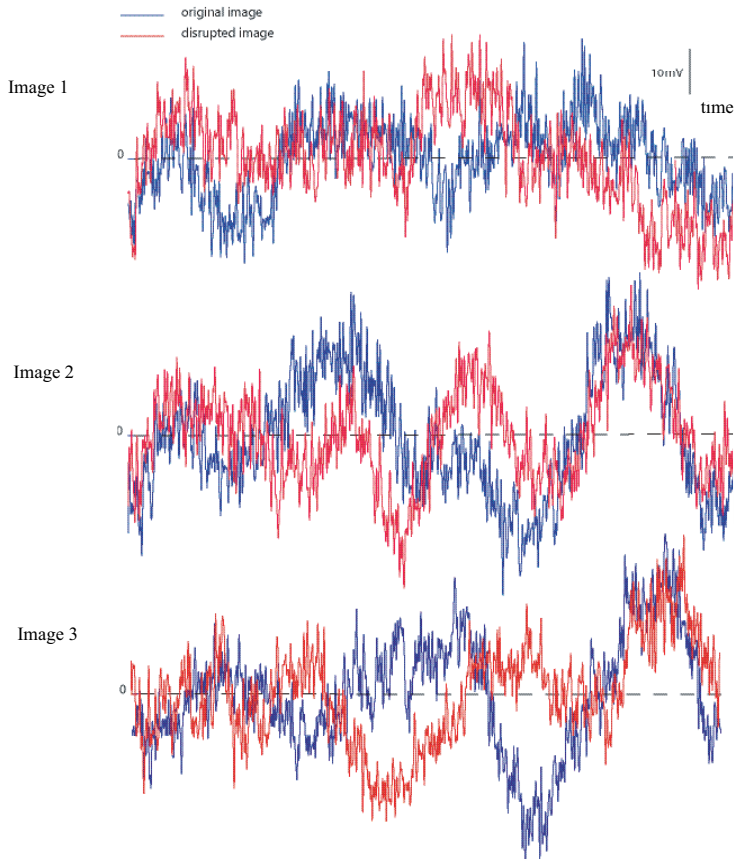

Figure 9.9. Comparison of physiological pattern noise of the original and disrupted images. The pattern noise for the three images of Figure 9.1 and also, for modified versions of these images (shown in Figure 9.6) where the vertical contours have been disrupted are shown. Notice that the pattern noise occurs for all images and that it is specific for each image. Comparing the original images with its modified versions, it can be seen that the pattern noise has changes. Peaks are typically reduced and often phase-shifted.

$\overline{R}$ is calculated by averaging the response of the wide field correlator at all points in the selected sampled space and sampled time. The relative error for the same set of responses is found by dividing their standard deviation by the mean. In this paper, the performance of the model is evaluated based on its effect on pattern noise.

Figure 9.11 shows the simulated phase aligned results superimposed with the physiological phase aligned fly response using Image 1. The phase aligned results are obtained by using a stimuli Image 1 moving at a speed of 180°/s at a contrast of 1. The c values give the cross covariance values obtained in each case and the 'error' values give the relative error measured in each case. The experiment is repeated with different models with saturation implemented at different places to compare the shapes of the curves obtained in each case. Figure 9.12 and Figure 9.13 shows simulated phase aligned results superimposed

Model	Image 1	Image 2	Image 3
no saturation	0.3785	0.3899	0.2506
only arm saturation	0.3301	0.2885	0.1100
only input saturation	0.3580	0.3030	0.1386
only output saturation	0.3723	0.4058	0.1503
input and arm saturation	0.3467	0.2585	0.1895
input and output saturation	0.3621	0.3908	0.0687
arm and output saturation	0.3594	0.2941	0.1037
all saturation	0.2433	0.2631	0.1539

Table 9.1. Cross covariance values for each model. From this table, it is clear that even though the results of saturation implemented at different positions when superimposed on each other shows a similarity with the physiological data, the cross covariance results tell us a different story. The model with no saturation implemented gives better covariance than models with saturation implemented at different positions. But for the Image 2, the model with just output saturation gives a good covariance value.

with the physiological phase aligned fly response using Image 2 and Image 3 respectively. The phase aligned results are obtained by using a stimuli Image 2 and Image 3 both moving at a speed of 180°/s at a contrast of 1. It is seen in all the three figures here that the model with no saturation implemented on it gives a better result than most of the saturated models. Only for Image 2 the model with just output saturation gives good covariance result. Though it is known that the saturation phenomena exist in the fly eye, and that it has an effect on the shape of pattern noise, the low covariance value shows that there are still more non-linearities present in the fly eye which the model has failed to capture. When the relative error is compared, it is seen that implementation of saturation decreases the relative error or pattern noise indicating addition of saturation helps in reducing pattern noise.

From the covariance Table 1, it is clear that even though the results of saturation implemented at different positions when superimposed on each other shows a similarity with the physiological data, the cross covariance results tell us a different story. The model with no saturation implemented gives better covariance than models with saturation implemented at different positions. But for the Image 2, the model with just output saturation gives a good covariance value.

Model	Image 1	Image 2	Image 3
no saturation	0.4445	0.4484	0.2553
only arm saturation	0.2754	0.3967	0.2826
only input saturation	0.3484	0.4634	0.1791
only output saturation	0.3714	0.3511	0.2128
input and arm saturation	0.1197	0.3503	0.3310
input and output saturation	0.2766	0.3598	0.2470
arm and output saturation	0.1894	0.3123	0.3275
all saturation	0.1784	0.2940	0.3266

Table 9.2. Relative error values for each model. From the table, it is clear models with no saturation give a higher relative error compared to models with saturation implemented. This is because of the greater difference in magnitude between the unsaturated response and the physiological data. Relative error actually measures the magnitude of the pattern noise and demonstrates that an unsaturated model has greater pattern noise than a model with all saturation. So in terms of relative error, saturation improves the model performance for images 1 and 2. For Image 3, which has the lowest contrast [Straw, 2004], it is seen that addition of saturation does not reduce pattern noise.

From the relative error Table 2, it is clear models with no saturation gives a higher relative error compared to models with saturation implemented. This is because of the greater difference in magnitude between the unsaturated response and the physiological data. Relative error actually measures the magnitude of the pattern noise and demonstrates that an unsaturated model has greater pattern noise than a model with all saturation. So in terms of relative error, saturation improves the model performance for images 1 and 2. For Image 3, which has the lowest contrast [Straw, 2004], it is seen that addition of saturation does not improve pattern noise. But when one compares the shape of the curves with the physiological data, to see if the peaks and troughs are seen at similar places as is tested using the cross covariance technique, it is found that the model with no saturation has more similarities than the one with saturation implemented.

In order to test the physiological data obtained, the first half of the data is correlated with the second half. In a perfect physiological recording this should give us a value very close to 1. But it is found that the self correlation results shows that physiological recording gives a lower value for the high contrast Image 1 compared to the low contrast Image 3 as seen in Table 3 which could be one reason why the model gives poor results [Rajesh et al., 2007].

Image 1 on itself	0.3380
Image 2 on itself	0.6169
Image 3 on itself	0.7359

Table 9.3. Cross correlation values obtained by correlating the first half of the image on the second half. In order to test the physiological data obtained, the first half of the data is correlated with the second half. In a perfect physiological recording this should give us a value very close to 1. But it is found that self correlation results shows that physiological recording gives a lower value for the high contrast Image 1 compared to the low contrast Image 3 as seen in this table which could be one reason why our model gives poor results.

Window size	Relative Error	Cross-Covariance
2×2	0.7018	0.1282
4×4	0.6954	0.1369
8×8	0.6669	0.1553
16×16	0.6320	0.1725
32×32	0.5980	0.1796

Table 9.4. Relative error and cross covariance values at different window size. Testing Image 2 with different window widths, increasing the window width from just 2×2 square window to a 32×32 square window, using the model with no saturation, the relative error and cross covariance in each case is calculated as shown in this Table. It is seen that relative error decreases as the window size increases and there is better covariance with larger windows than there is with small window size showing that larger window of EMDs gives better results than small windows.

Testing Image 2 with different window widths, increasing the window width from just 2×2 square window to a 32×32 square window, using the model with no saturation, the relative error and cross covariance in each case is calculated as shown in the Table 4. It is seen that relative error decreases as the window size increases and there is better covariance with larger windows than there is with small window size showing that larger window of EMDs gives better results than small windows.

9.5 Conclusion

In this chapter, the pattern noise present in HS cell response is studied and an attempt is made to reproduce pattern noise seen in the fly response using natural images with our model. The addition of static compressive non-linearity at different places in the model has been found to have a significant affect on the shape of the pattern noise and it is likely that saturation has a role in affecting pattern noise in the fly motion detector. Though initial results show that there could be a match between modelling and physiological results, proper scaling and calculation of cross covariance showed that the model with no saturation seemed to give better result. But it is found from the self correlation results that physiological recording gives a lower value for the high contrast Image 1 compared to the low contrast Image 3 which could be one reason why our model gives poor results.Though it is known that the saturation phenomena exist in the fly eye, and that it has an effect on the shape of pattern noise, the low covariance value shows that there are still more non-linearities present in the fly eye which the model has failed to capture. It is also noted that better covariance results can be obtained by increasing the window size to include larger EMDs. The relative error results in this Chapter tell us a different story. Relative error actually measures the magnitude of the pattern noise and demonstrates here that an unsaturated model has greater pattern noise than a model with all saturation.

In nature, pattern noise is due to the response of local motion detectors to image features. It is largely reduced by the horizontally extended receptive field of HS cells and by summation at the steering muscles. Though our model is not able to exactly mimic the fly visual properties, it is able to reproduce this phenomenon faithfully to a large extent and hence can be used to study the impact of pattern noise on artificial motion detectors. In the next chapter, a small 16 pixel yaw sensor is modelled using our elaborated model.

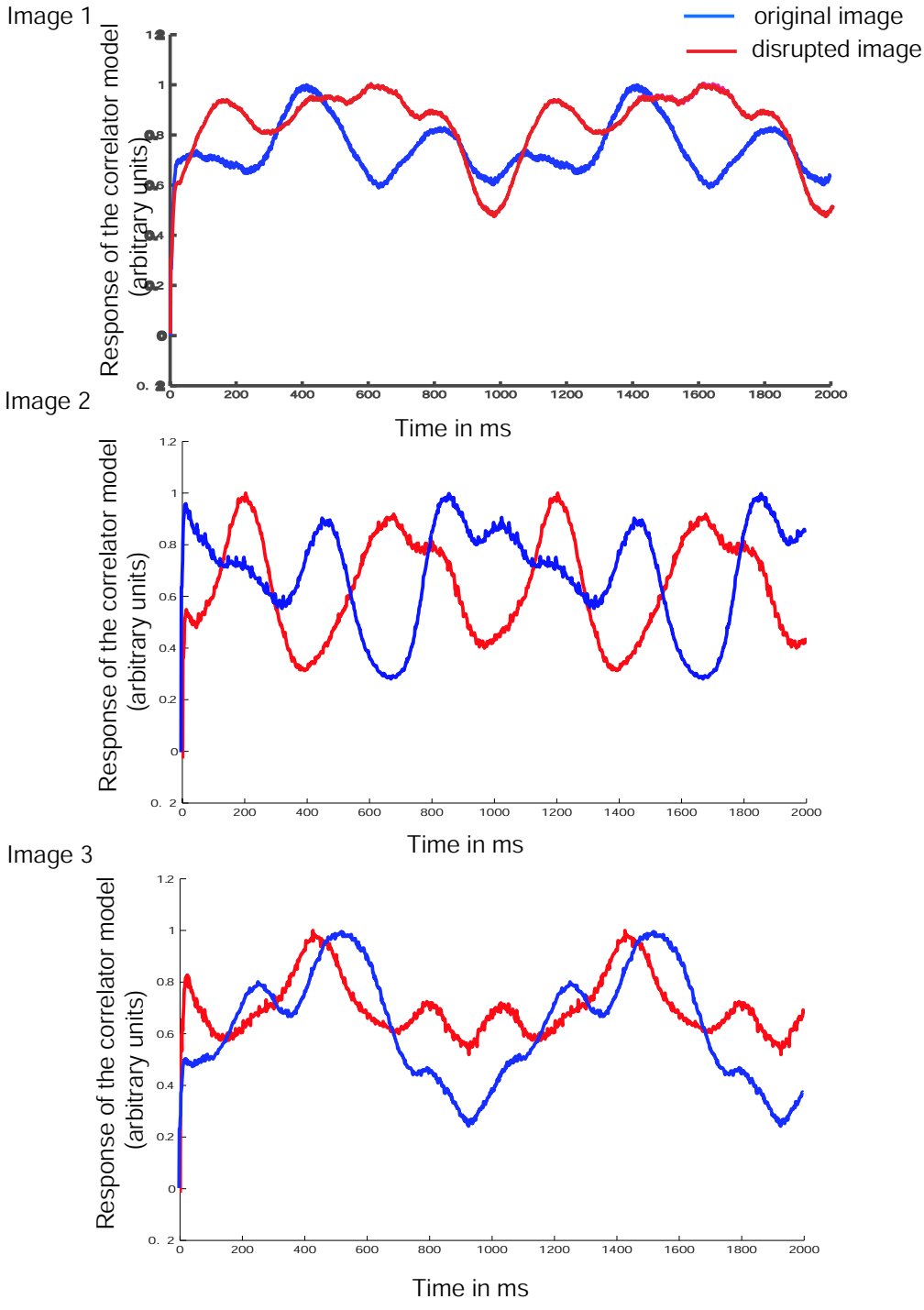

Figure 9.10. Comparison of simulated pattern noise of the original and disrupted images. Pattern noise results for three different images and for the modified versions of these images obtained by simulating our elaborated Reichardt model. It can be seen that pattern noise occurs for all images and it is different for different images. Comparing the original image with its modified versions, it can be seen that like in the physiological data, the pattern noise has changes and the shifted counterparts show phase-shifts in their response.

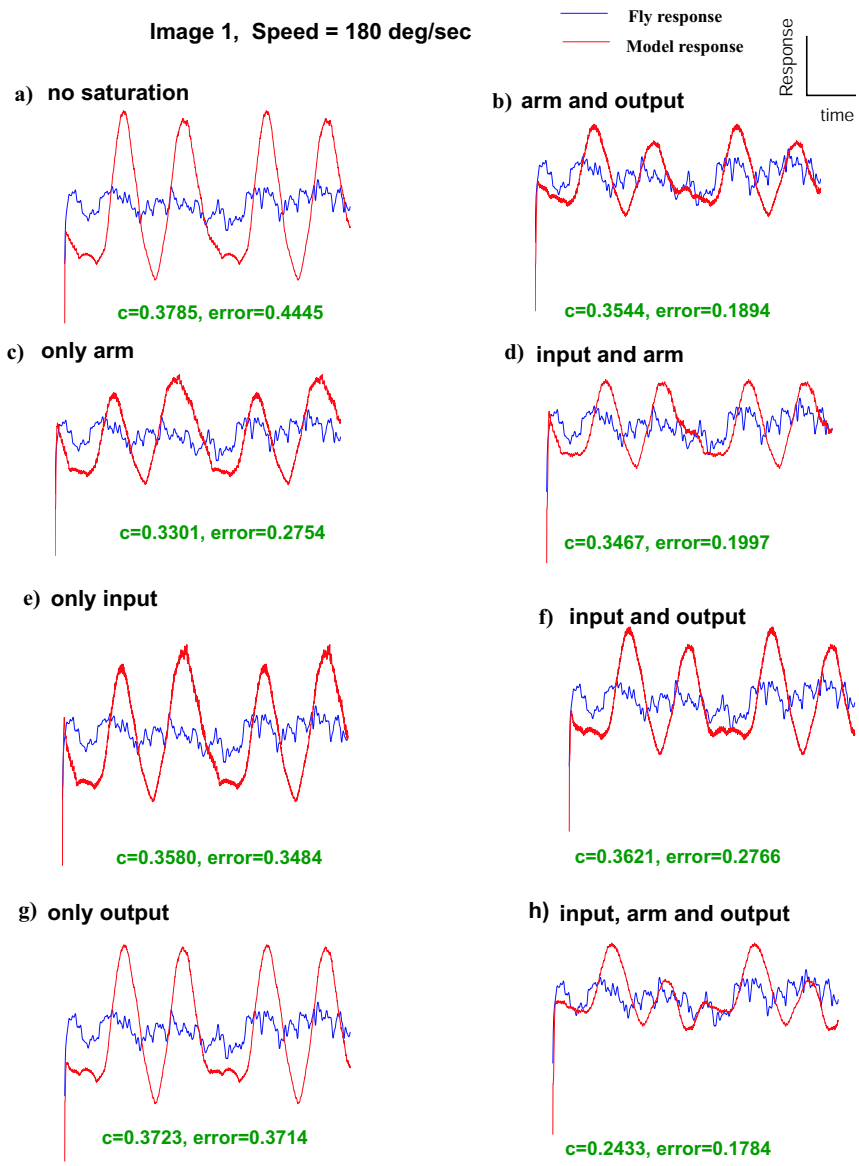

Figure 9.11. Simulated phase aligned results superimposed with the physiological phase aligned fly response using Image 1. The phase aligned results are obtained by using a stimuli Image 1 moving at a speed of $180^{\circ}/s$ at a contrast of 1. The c values give the cross covariance values obtained in each case and the 'error' values give the relative error measured in each case. The experiment is repeated with different models with saturation implemented at different places to compare the shapes of the curves obtained in each case. It is seen that the model with no saturation implemented on it gives the best covariance value. Though it is known that saturation phenomena exist in the fly eye, and that it has an effect on the shape of pattern noise, the low covariance value shows that there are still more non-linearities present in the fly eye which the model has failed to capture. When the relative error is compared, it is seen that implementation of saturation decreases the relative error or pattern noise indicating addition of saturation helps in reducing pattern noise.

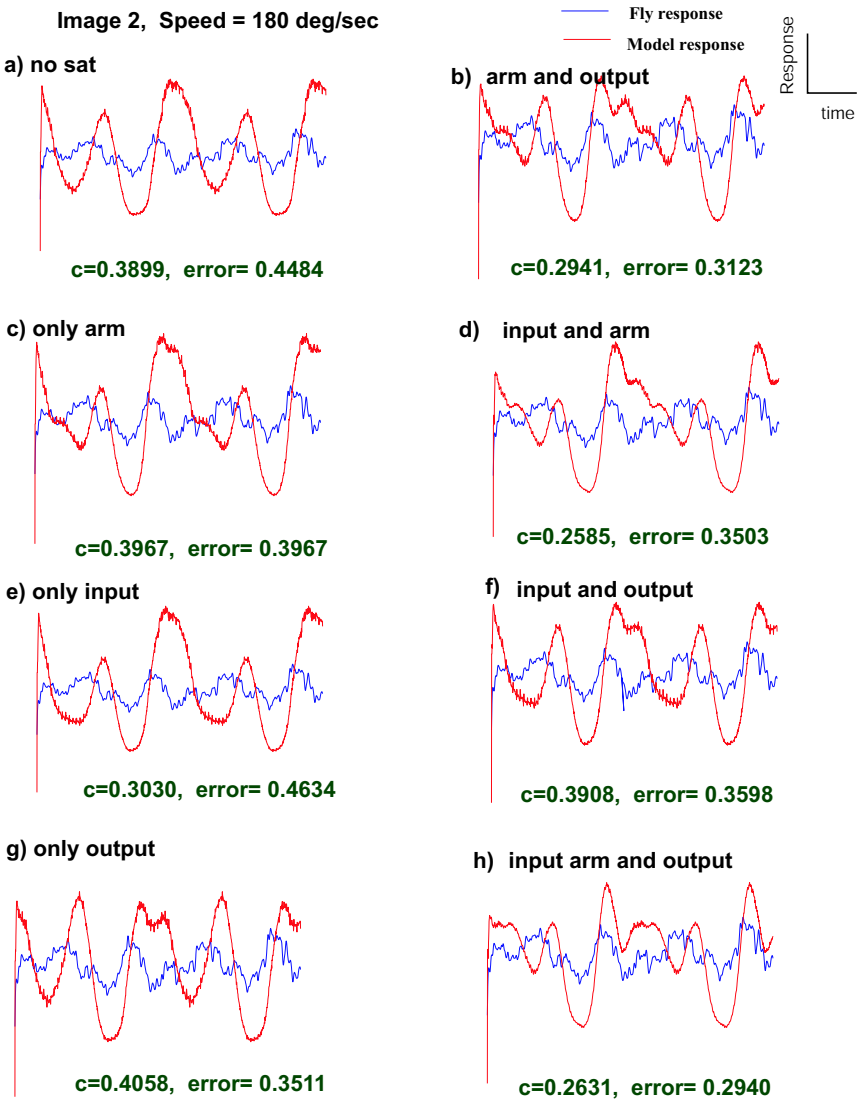

Figure 9.12. Simulated phase aligned results superimposed with the physiological phase aligned fly response using Image 2. The phase aligned results are obtained by using a stimuli Image 2 moving at a speed of $180^\circ/s$ at a contrast of 1. The c values give the cross covariance values obtained in each case and the 'error' values give the relative error measured in each case. The experiment is repeated with different models with saturation implemented at different places to compare the shapes of the curves obtained in each case. It is seen that the model with no saturation implemented on it gives a better result than most of the saturated models. Though it is known that the saturation phenomena exist in the fly eye, and that it has an effect on the shape of pattern noise, the low covariance value shows that there are still more non-linearities present in the fly eye which the model has failed to capture. When the relative error is compared, it is seen that implementation of saturation decreases the relative error or pattern noise indicating addition of saturation helps in reducing pattern noise.

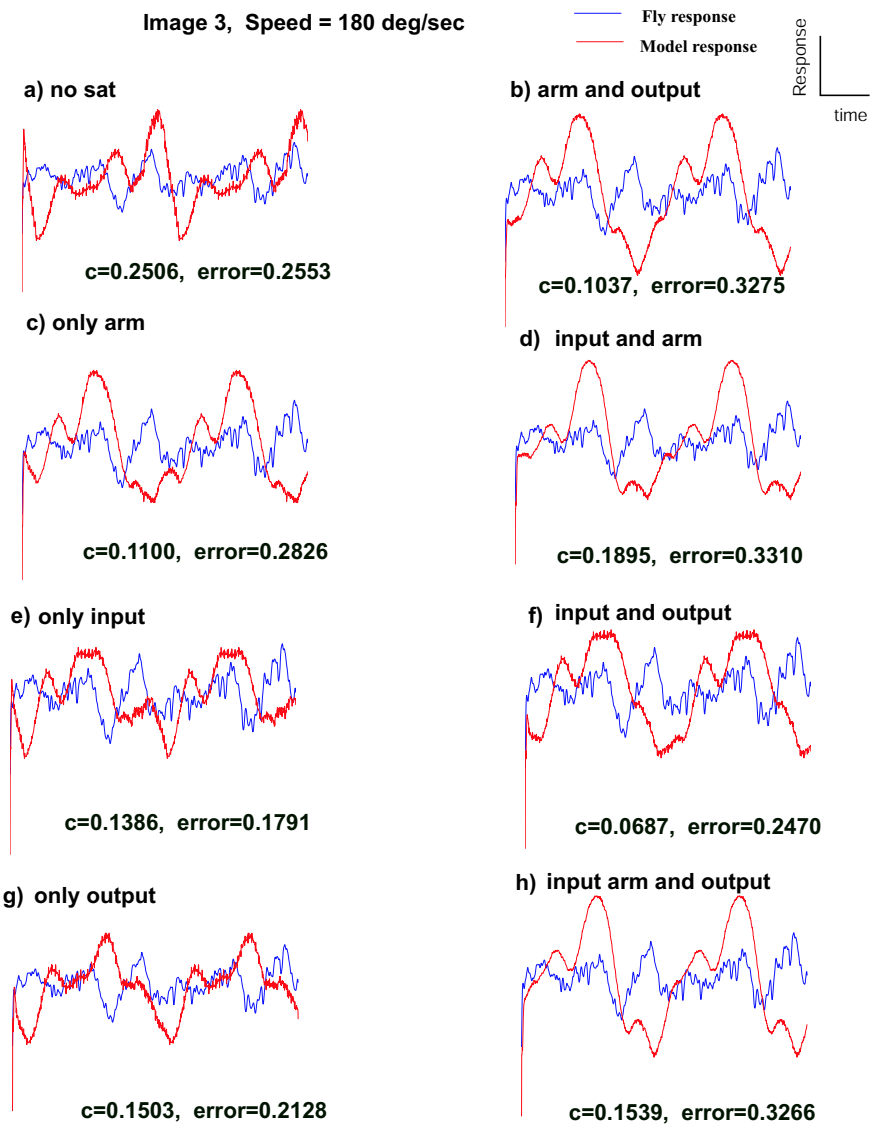

Figure 9.13. Simulated phase aligned results superimposed with the physiological phase aligned fly response using Image 3. The phase aligned results are obtained by using a stimuli Image 3 moving at a speed of 180°/s at a contrast of 1. The c values give the cross covariance values obtained in each case and the 'error' values give the relative error measured in each case. The experiment is repeated with different models with saturation implemented at different places to compare the shapes of the curves obtained in each case. It is seen that the model with no saturation implemented on it gives the best covariance results. Though it is known that the saturation phenomena exist in the fly eye, and that it has an effect on the shape of pattern noise, the low covariance value shows that there are still more non-linearities present in the fly eye which the model has failed to capture. When relative error is compared, it is seen that only for this image, which has the lowest aggregated natural contrast [Straw, 2004] when compared to the other two images, the error values have not improved with the addition of saturation.